Investigation of the Binding of Isoform-Selective Inhibitors to Prostaglandin Endoperoxide Synthases Using Fluorescence Spectroscopy†

Cheryl A. Lanzo,‡ Joseph M. Beechem,§ John Talley,|| and Lawrence J. Marnett*,‡

A. B. Hancock, Jr., Memorial Laboratory for Cancer Research, Departments of Biochemistry and Chemistry, and Department of Molecular Physiology and Biophysics, Vanderbilt University School of Medicine, Nashville, Tennessee 37232, and Department of Inflammatory Disease Research, Searle Research and Development, St. Louis, Missouri 63198-0001

Received July 11, 1997; Revised Manuscript Received September 15, 1997⊗

ABSTRACT: Prostaglandin endoperoxide synthase (PGHS) is a heme protein that catalyzes the committed step in prostaglandin and thromboxane biosynthesis. Two isoforms of PGHS exist, a constitutive form termed PGHS-1 and an inducible form termed PGHS-2. We report here fluorescence resonance energy transfer analysis of isoform-selective inhibitors interacting with PGHS-1 and PGHS-2. By measuring fluorescence quenching due to the energy transfer of the inhibitor fluorescence to the heme prosthetic group of PGHS, we determined these inhibitors bind in the arachidonic acid substrate access channel with an R_0 of 35 Å for PGHS-1 with the PGHS-1 inhibitor and an R_0 of 21 Å for PGHS-2 with the PGHS-2 inhibitor. The observed fluorescence quenching is completely dynamic and dominated by quenching by the heme. Time-resolved results combined with molecular modeling determine the distance from the inhibitor to the heme moiety to be 20 Å in PGHS-1 and 18 Å in PGHS-2. Preliminary stopped-flow kinetic studies reveal that the rate of quenching is limited by a first-order protein transition, which is slow, and that bound inhibitor undergoes rapid exchange.

Prostaglandin endoperoxide synthase (PGHS)[1] catalyzes the committed step in prostaglandin and thromboxane biosynthesis (*1*−*3*). The combined action of its cyclooxygenase and peroxidase activities convert arachidonic acid into PGH_2, the immediate precursor of PGD_2, PGE_2, $PGF_{2\alpha}$, PGI_2, and TxA_2 (*4, 5*). Two PGHS isoforms exist in human and animal tissue. PGHS-1 is normally expressed constitutively, whereas PGHS-2 is inducible and short-lived (*6*−*8*). PGHS-2 expression is stimulated by growth factors and cytokines and inhibited by glucocorticoids (*6, 7, 9, 10*). PGHS-1 appears to be responsible for the synthesis of cytoprotective prostaglandins in the stomach and thromboxane in platelets, whereas PGHS-2 is a major contributor to prostaglandin synthesis in inflammatory cells and the brain (*11, 12*).

Inhibition of the cyclooxygenase activity of PGHS is the principal mechanism of action of nonsteroidal antiinflammatory drugs (NSAIDs) (*13*). All currently available NSAIDs inhibit both PGHS isoforms to varying degrees (*14, 15*). On the basis of the tissue distribution of the two isoforms, selective inhibition of PGHS-2 should alleviate the symptoms of inflammation and pain without the gastrointestinal and vascular effects exhibited by PGHS-1 inhibitors. Several selective PGHS-2 inhibitors have been developed and, indeed, have been found to be antiinflammatory and analgesic but nonulcerogenic (Figure 1) (*11, 16, 17*). Among these PGHS-2 selective inhibitors are a series of diarylheterocycles such as DuP697 and related molecules.

Diarylheterocycles have been extensively investigated as selective PGHS inhibitors (*18, 19*). These compounds are structurally distinct from the arylaliphatic acids that constitute the majority of commercially successful NSAIDs. An intriguing finding from structure−activity studies is that the selectivity of PGHS-1 or PGHS-2 inhibition by several sulfur-substituted diarylheterocycles depends on the oxidation state of the sulfur atom. For example, SC58076 selectively inhibits PGHS-1 with a K_i of 0.2 μM and k_{inact} of 0.03 s^{-1}, whereas SC58092 selectively inhibits PGHS-2 with a K_i of 1 μM and k_{inact} of 0.1 s^{-1} (eq 1) (*20, 21*).

The three-dimensional structure of PGHS-1 has been solved at 3.5 Å resolution by X-ray analysis of cocrystals of the enzyme with one of several arylaliphatic acid inhibitors (*22, 23*). Each structure demonstrates that the inhibitor is bound in the arachidonic acid access channel with its carboxylate group ion-paired to Arg120. Mutation of Arg120 reduces the potency of arylaliphatic acids as cyclooxygenase inhibitors yet does not lower the inhibitory potency of diarylheterocycles (*24, 25*).

† This work was supported by research grants from the National Institutes of Health (CA47479, GM45990, RR5823) and an NIEHS training grant to C.A.L. (ES07028).

* To whom correspondence should be addressed. Tel. (615) 343-7329; Fax (615) 343-7534; E-mail marnett@toxicology.mc.vanderbilt.edu.

‡ A. B. Hancock, Jr., Memorial Laboratory for Cancer Research, Departments of Biochemistry and Chemistry, Vanderbilt University School of Medicine.

§ Department of Molecular Physiology and Biophysics, Vanderbilt University School of Medicine.

|| Searle Research and Development.

⊗ Abstract published in *Advance ACS Abstracts,* November 15, 1997.

[1] Abbreviations: PGHS, prostaglandin endoperoxide synthase (EC 1.14.99.1); NSAID, nonsteroidal antiinflammatory drug; SC58076, 2-(2-chlorophenyl)-4-[4-(methyl mercapto)phenyl]-5-[4-(methoxy)phenyl]-thiazole; SC58092, 2-(2-chlorophenyl)-4-[4-(methylsulfonyl)phenyl]-5-[4-(methoxy)phenyl]thiazole; DuP 697, 5-bromo-2-(4-fluorophenyl)-3-[4-(methylsulfonyl)phenyl]thiophene; TRFS, time-resolved fluorescence spectroscopy; FRET, fluorescence resonance energy transfer.

S0006-2960(97)01691-7 CCC: $15.00
Published on Web 01/06/1998

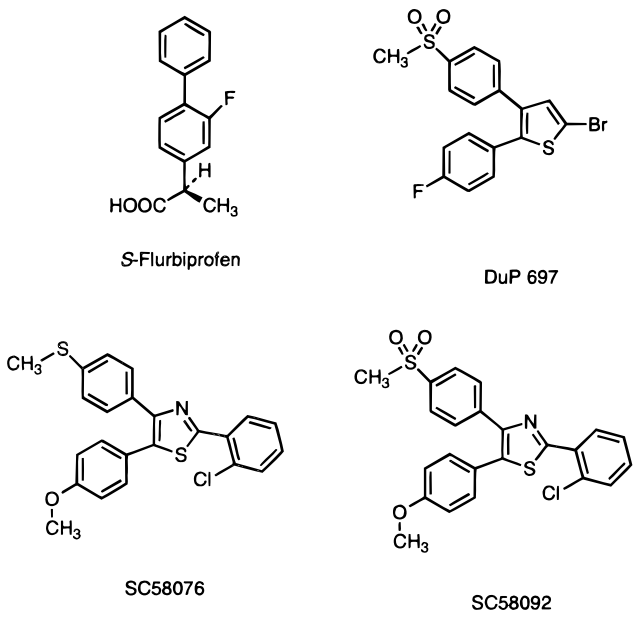

FIGURE 1: Chemical structures of PGHS inhibitors.

Recently, the crystal structures of PGHS-2 complexed with different inhibitors have also been solved (*26*, *27*). These structures show that the PGHS-2 structure is very similar to the PGHS-1 structure. The main difference in PGHS-2 is that the arachidonic acid binding site is larger due to a Val at position 523, which is an Ile in PGHS-1. The reduced size of the Val residue opens up a pocket in which the sulfonamide moiety of the selective PGHS-2 inhibitor binds. Site-directed mutagensis of Val523Ile in PGHS-2 results in a PGHS-2 mutant that is selectively inhibited by PGHS-1-selective inhibitors (*28*).

We have employed fluorescence spectroscopy as a dynamic probe of the interaction of PGHS with isoform-selective inhibitors in solution. The diarylthiazoles SC58076 and SC58092 differ only in the oxidation state of the sulfur atom, but SC58076 is a PGHS-1-selective inhibitor and SC58092 is a PGHS-2-selective inhibitor (Figure 1). Both compounds are fluorescent and display very similar fluorescence spectra, which makes them useful probes for studying their selectivity of binding to PGHS-1 and PGHS-2. The fluorescence emission spectra of SC58076 and SC58092 both overlap with the strong heme absorption of PGHS. This large overlap results in a very strong quenching of the bound inhibitor upon interaction with PGHS-1 and PGHS-2. The present report describes the results of fluorescence resonance energy transfer (FRET) and time-resolved experiments that demonstrate the utility of fluorescence techniques for studying the PGHS−inhibitor interactions and provide an estimate of the position of the inhibitors in the arachidonate binding channel of sheep PGHS-1 and human PGHS-2.

MATERIALS AND METHODS

Materials. Arachidonic acid was purchased from Nu Chek Prep (Elysian, MN). Hematin was purchased from Sigma Chemical Co. (St. Louis, MO). *S*-Flurbiprofen was provided by the Upjohn Co. (Kalamazoo, MI). Ram seminal vesicles were purchased from Oxford Biomedical Research, Inc. (Oxford, MI). PGHS-1 was purified from ram seminal vesicles as described earlier (*29*). Protein concentrations were determined by the Bio-Rad dye binding assay using a BSA standard for PGHS-1 and then multiplying by 1.5. This factor was previously determined by amino acid analysis of purified PGHS-1. The protein had a specific activity of 20 μmol of arachidonic acid min^{-1} mg^{-1} and the percentage of holoenzyme was 18%. Apo PGHS-1 was prepared as described earlier (*30*). Human PGHS-2 was kindly provided by J. Gierse (Monsanto, St. Louis, MO) with a specific activity of 16 μmol of arachidonic acid min^{-1} mg^{-1} and holoenzyme content of 2%. Holo-PGHS-1 or PGHS-2 used in all the experiments was prepared from apoproteins by adding heme in a 1:1 ratio. Heme was prepared by dissolution in dimethyl sulfoxide.

Steady-State Fluorescence Emission Spectra. Steady-state emission spectra were obtained with a Spex 1681 Fluorolog spectrofluorometer, equipped with a 450 W xenon arc lamp. Technical, noncorrected, fluorescence emission spectra were collected from 380 to 550 nm by exciting samples at 340 nm for SC58076 and 346 nm for SC58092. Quinine sulfate was utilized for quantum yield determinations, $Q = 0.51$. Since the quinine emission spectra were nearly identical to those of the inhibitors, noncorrected spectra were used. The excitation and emission bandwidths were 1−2 nm for all the spectra. Background fluorescence from buffer alone, apoprotein, or holoprotein was recorded and subtracted from the samples containing SC58076 or SC58092 unless otherwise noted. Steady-state measurements were performed at room temperature in a 1 mL fluorescence cuvette with 10 mm excitation and 2 mm emission path lengths. Both fluorophores were dissolved in acetonitrile before further dilution into buffer. The organic component of the fluorophores in buffer was kept below 8% when in the presence of protein.

Time-Resolved Fluorescence Instrument and Measurements. Time-resolved fluorescence measurements at equilibrium were performed by utilizing a frequency-doubled Coherent Mira 900-F titanium sapphire laser pumped by a Coherent Innova 304 argon ion laser (Santa Clara, CA). Output pulses from this laser at 365 nm were utilized at 4 MHz and had a pulse width of approximately 150 fs. A half-wave plate in the excitation beam was utilized to rotate the excitation polarization to horizontal for the determination of the polarization bias (*G* factor) for the detection instrumentation. The fluorescence emission signal was passed through a Glan-Thompson polarizer and a Hoya 440 cuton filter (Fremont, CA) and focused into a ISA HR320 (Edison, NJ) 0.33-m emission monochromator set at 461 nm (bandwidth 8 nm). The fluorescence emission was detected by a 6 μm microchannel plate detector (Hamamatsu R3809U-01, Bridgewater, NJ) operating in time-correlated single photon counting mode. The impulse response functions were typically 30−50 ps full width at height maximum. Timing calibration was 12 ps/channel with data collected into 2500−3000 channels. Typical total intensity sum curves had approximately 50 000 counts in the peak channel. Time-resolved measurements were performed on 200 μL samples in cuvettes with 3 × 3 mm path length. Protein solutions (2 μM) were prepared in 80 mM Tris/HCl, pH 8.0. The measurements were taken at room temperature. During acquisitions, the emission polarizer rotated from vertical to horizontal every 30 s (30 s vertical, $I_\perp$, and 30 s horizontal,

$I_{||}$, each), to measure the parallel and perpendicular components of the emission.

DATA ANALYSIS

Time-Resolved Anisotropy Decays. Fluorescence anisotropy decays of inhibitor only, inhibitor bound to apoprotein (donor) and inhibitor bound to holoprotein (acceptor) were used to study the rotation of the inhibitor bound versus unbound. Anisotropy decays, $r(t)$, were described as

$$r(t) = \sum_{i=1} \beta_i \exp(-t/\phi_i)$$

where β_i is the amplitude of the motion associated with the component of the decay and ϕ_i is the rotational correlation time. Longer correlation times are associated with the global overall motion of the protein, and the shorter components represent the inhibitor's local motion. Depolarization factors for the inhibitors were determined from the time-resolved anisotropy decays and from the fundamental anisotropy values (see below for κ^2).

Simultaneous analysis of the two polarized components of the emission, $I_\perp$ and $I_{||}$, was performed using the GLOBALS UNLIMITED software package (*31*). Goodness of the fit was judged by examination of χ^2 and the residuals distribution.

Measurements of Energy Transfer: Calculation of the Forster Distance. The Forster distance, R_0, is the separation for 50% efficiency of resonance energy transfer. R_0 is related to the spectroscopic properties of the donor (apoprotein bound to inhibitor) and acceptor (holoprotein bound to inhibitor). Two approaches were taken to calculate R_0, steady-state analysis and time-resolved analysis. For steady-state:

$$R_0 = 0.211(Jn^{-4}Q_D\kappa^2)^{1/6}$$

where J (M^{-1} cm^{-1} nm^4) is the spectral overlap between the emission spectrum of the donor and the absorption spectrum of the acceptor. J was approximated by

$$J = \sum F_D(\lambda)\epsilon_A(\lambda)\lambda^4\,\Delta\lambda$$

where $F_D(\lambda)$ is the normalized (to unit area) emission spectrum of the donor sample, $\epsilon(\lambda)$ is the absorption spectrum (M^{-1} cm^{-1}) of the acceptor from the donor−acceptor samples, and n is the refractive index of the medium between the donor and the acceptor, approximated as 1.4 for all the samples. Q_D is the fluorescence quantum yield of the donor samples. Q_D was determined for the donor sample using a reference of quinine bisulfate in 0.1 N H_2SO_4, using a quantum yield for quinine of 0.51 (*44*).

The distance from the fluorophore to the acceptor, R, is determined by

$$R = R_0\left(\frac{1-E}{E}\right)^{1/6}$$

where E is the energy transfer efficiency defined by

$$E = 1 - \frac{Q_{DA}}{Q_D}$$

where Q_{DA} is the fluorescence quantum yield of the donor in the presence of the acceptor and Q_D is as defined above.

Estimation of κ^2. κ^2 is the orientation factor, the value of which depends on the relative orientation of the transition dipoles of the donor and acceptor and the line between the donor and acceptor. The PGHS-1 crystal structure reveals an internal channel that has been found to be the binding site for many cyclooxygenase inhibitors. Therefore a better estimate of κ^2 was derived by "placing" the inhibitor into the access channel. Molecular modeling was then performed using just steric constraints using INSIGHTII with the Builder, Docking, and Discover modules. Coordinates of PGHS-1 were generously provided by R. M. Garavito. SC58076 was docked in the substrate access channel of PGHS-1 and energy-minimized. The coordinates for the heme and SC58076 were taken from this energy-minimized structure and κ^2 was estimated according to

$$\kappa^2 = {}^1/_2\{1 + 3(\hat{d}+\hat{r})^2 - [\hat{d}\cdot\hat{n}_A - 3(\hat{d}+\hat{r})^2(\hat{r}\cdot\hat{n}_A)]^2\}$$

where d is the donor transition moment, r is the line between the donor and acceptor, and n is the normal to the plane of the acceptor (heme). The orientation of the donor emission oscillator was modeled using the same direction as the closely related stilbene class of fluorophores (*32*, *33*).

Time-Resolved Energy Transfer Analysis (Empirical Exponential Analysis). Inhibitor free in solution or bound to apo- or holo-PGHS presents complex intensity decays. Determination of the average energy-transfer efficiencies, $\langle E\rangle$, was done from the ratio of the average lifetimes of the inhibitor bound to apo-PGHS (donor), $\langle\tau_D\rangle$, and the inhibitor bound to holo-PGHS (acceptor), $\langle\tau_{DA}\rangle$, calculated from a least-squares arbitrary multiexponential fitting procedure. The donor-only decay is given by

$$I_D(t) = I_D^0\sum \alpha_i \exp(-t/\tau_{Di})$$

where I_D^0 is the total donor intensity at $t = 0$. And the average donor lifetime, $\langle\tau_D\rangle$, is given by

$$\langle\tau_D\rangle = \sum_{i=1}^{n}\alpha_i\tau_{Di}/\sum_{i=1}^{n}\alpha_i$$

α_i and τ_{Di} are the amplitude and lifetime, respectively, of the ith component. Three lifetimes are required for adequate fitting for the donor-only and donor-acceptor. The fluorescence decay of the donor-acceptor pair was also empirically analyzed by multiexponentials. This analysis gave the average $\langle\tau_{DA}\rangle$. The energy transfer efficiency was calculated by $\langle E\rangle = 1-\langle\tau_{DA}\rangle/\langle\tau_D\rangle$. Since $\langle\tau_{DA}\rangle$ and $\langle\tau_D\rangle$ are obtained without the need of absolute protein concentrations, uncertainties associated with protein concentration determinations are eliminated by time-resolved fluorescence measurements. Time-resolved fluorescence data analysis was performed using the GLOBALS UNLIMITED software package (*31*).

Stopped-Flow S-Flurbiprofen Competititon of SC58076 Preloaded on PGHS-1. Reactions were performed with an SFM-3 stopped-flow unit (Molecular Kinetics, Pullman, WA) with a 100 μL FC.15 fluorescence cuvette and hard-stop shutter. Reaction flow rates were 4−8 mL/s. Reaction time bases depended on the experiment. Extensively degassed stock solutions of PGHS-1 alone or PGHS-1 preloaded with

SC58076, *S*-flurbiprofen, SC58076, and reaction buffer were loaded into separate syringes. All experiments were performed at ambient temperature and were collected with a fraction of the data channels devoted to internal controls. The internal controls for the on rate were SC58076 alone. The internal controls for the competition experiments were protein prebound to inhibitor. These control reactions were used to normalize the observed total intensity change of the reaction.

A T-format polarized steady-state stopped-flow detection was utilized. The excitation beam was a 450 W xenon arc lamp with a 0.22 m SPEX monochromator (Edison, NJ) whose output was focused onto a fused-silica fiber optic (10 × 100 mm fiber bundle) and directed into a 100 μL stopped-flow cuvette. On each side of the SFM-3 cuvette head, an emission channel was mounted, consisting of a collimating lens, polarizer, and 440 nm filter. The fluorescence emission was measured by PMTs operating in single-photon counting mode with multichannel scaling (Tennelec MCS2, Oak Ridge TN). Multiple runs were summed to obtain adequate signal to noise ratios. The data were analyzed with the GLOBALS UNLIMITED software package using a nonlinear least-squares algorithm.

RESULTS

Steady-State Analysis of the Quenching of SC58076 Fluorescence by PGHS-1. The interaction of most inhibitors with PGHS can be described by the two step mechanism depicted in eq 1. Enzyme and inhibitor rapidly combine to form a reversible complex, EI, that undergoes a relatively slow transformation to a second complex, EI*, in which the inhibitor is bound more tightly to the enzyme. The second complex is non-covalent for most inhibitors but its formation is believed to be only slowly reversible. The formation of the tightly bound complex is responsible for the selectivity of inhibition of PGHS-1 or PGHS-2 by diaryl heterocycles (*34*).

$$\mathrm{E} + \mathrm{I} \underset{k_{-1}}{\overset{k_1}{\rightleftharpoons}} [\mathrm{E}\cdot\mathrm{I}] \xrightarrow{k_2} [\mathrm{E}\cdot\mathrm{I}]^* \qquad (1)$$

$$K_\mathrm{i} = k_{-1}/k_1 \qquad k_\mathrm{inact} = (k_{-1} + k_2)/k_1$$

The kinetic parameters that describe the interaction of SC58076 with PGHS-1 have been determined previously to be $K_\mathrm{i} = 0.2$ μM and $k_\mathrm{inact} = 0.03$ s^{-1} (*21*). For steady-state fluorescence energy transfer experiments, the inhibitors were incubated with the enzyme for 15 min before the fluorescence spectra were recorded so the measurements should reflect the tightly bound inhibitor−enzyme complexes.

The emission spectra of SC58076 and SC58092 in acetonitrile reveals SC58076 is 50% more fluorescent than SC58092, but the similarity of both spectra indicate that the chromophores and fluorophores are very similar in the two molecules. The λ_max of SC58076 and SC58092 are 450 and 455 nm, respectively. Figure 2 depicts the fluorescence spectra of SC58076 (1 μM) following its incubation with apo- and holo-PGHS-1 (4 μM). The λ_max of SC58076 after incubation with apo- or holo-PGHS-1 red-shifts to 458 nm. The fluorescence intensity of SC58076 incubated with apoprotein increased relative to inhibitor in solution (not shown). In contrast, the fluorescence intensity of SC58076 when incubated with holoprotein was reduced by 80−90% relative to inhibitor bound to apoprotein.

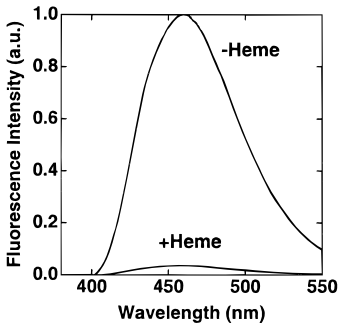

FIGURE 2: Steady-state fluorescence spectroscopy of holo- and apo-PGHS-1 bound to SC58076. PGHS-1 (4 μM) was reconstituted with 1 equiv of heme or an equal volume of dimethyl sulfoxide to generate holo- and apoenzyme, respectively. SC58076 (1 μM) was added and the fluorescence emission spectra were recorded as described in Materials and Methods. Buffer background was subtracted.

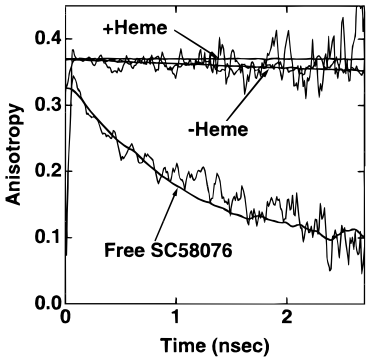

FIGURE 3: Time-resolved anisotropies of free SC58076 and SC58076 with apo- and holo-PGHS-1. PGHS-1 (2 μM) was incubated with 500 nM SC58076 before the addition of 2 μM heme in DMSO or DMSO vehicle. Time-resolved measurements were performed as described in Materials and Methods. Anisotropies were determined as described in the analysis.

Time-Resolved Anisotropy Analysis of the Binding of SC58076 to PGHS-1. The quenching in fluorescence observed on incubation of SC58076 with holo-PGHS-1 was consistent with fluorescence energy transfer to the heme prosthetic group of the enzyme. The absence of fluorescence quenching in the apoenzyme, however, may indicate poor binding to the apoenzyme. To test this, the binding of SC58076 to apo- and holo-PGHS-1 was probed with time-resolved fluorescence anisotropy experiments, which can clearly distinguish bound from free ligands by their rotational properties.

Apo- and holo-PGHS-1 (2 μM) were incubated with SC58076 (500 nM). Time-resolved measurements were taken after these samples were allowed to reach equilibrium. Analysis of the time-resolved anisotropy demonstrated that SC58076 bound to both apo- and holo-PGHS-1 (Figure 3). SC58076, dissolved in solution, has a rapid correlation time of 2.9 ns that was not affected by adding free hematin (data not shown). In contrast, when apo- or holo-PGHS-1 was added to SC58076, the rotational correlation time of SC58076 increased to approximately 180 ns. This long rotational correlation time clearly indicates SC58076 binding to both apoenzyme and holoenzyme.

Time-Resolved Analysis of SC58076 Bound to Apo-PGHS-1 and Titrated with Heme. The heme prosthetic group

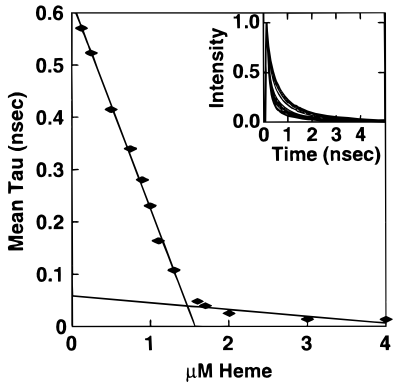

FIGURE 4: Average fluorescence lifetime of SC58076 with apo-PGHS-1 titrated with heme. Apo-PGHS-1 (2 μM) was incubated with 500 nM SC58076 before the addition of 0−4 μM heme. Time-resolved measurements were taken as described in Materials and Methods. Seventy-five percent of PGHS-1 was capable of binding heme and quenching SC58076 as determined by the fits generated through the mean τ vs micromolar heme data. The inset displays the normalized intensities of the time-resolved measurements; the lifetimes decrease with increasing heme. The mean τ was determined as described in Materials and Methods.

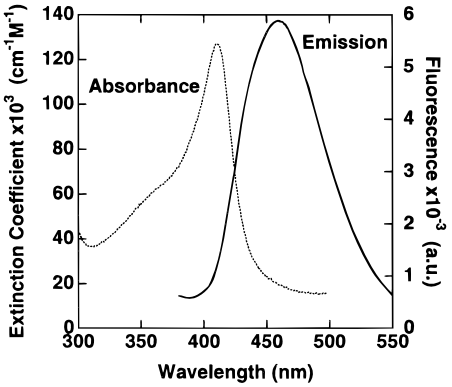

FIGURE 5: Region of spectral overlap between SC58076 bound to apo-PGHS-1 (donor) and holo-PGHS-1 (acceptor). Absorbance and emission spectra were taken as described in Materials and Methods.

of PGHS is easily removed by gel filtration to generate apoenzyme. In turn, the apoenzyme can be easily reconstituted with heme to regenerate holoenzyme. To determine what percentage of the enzyme was capable of binding and quenching SC58076 and to further demonstrate that heme is the fluorescence resonance energy transfer acceptor of SC58076, time-resolved measurements of a heme titration of apo-PGHS-1 prebound to SC58076 were performed.

The fluorescence lifetime of SC58076 decreased when heme was titrated into apo-PGHS prebound to SC58076 (Figure 4, inset). Figure 4 shows the average fluorescence lifetime of the bound SC58076 versus heme concentration. SC58076 bound to apo-PGHS-1 had an average fluorescence lifetime of 0.66 ns. In sharp contrast, SC58076 bound to holo-PGHS-1, fully reconstituted with heme, was strongly quenched and had an average lifetime of 0.024 ns. The efficiency of SC58076 energy transfer to the heme of holoprotein calculated from the fluorescence lifetime is approximately 96%. In addition, the heme titration allowed the determination of the percent of apoprotein capable of binding heme and quenching the fluorescence as 75%. This correlates well with the percentage of heme binding determined from activity titrations. Previous experiments have shown that apo-PGHS-1, prepared by the procedures described, is capable of binding 70−80% of theoretical heme per subunit (*20*). The remaining 20−30% of protein represents denatured protein molecules that do not bind heme (*20*, *35*). Denatured protein also does not bind diarylheterocycles so SC58076 can only bind to and be quenched by the reconstituted holoenzyme.[2] The holoenzyme was in excess over SC58076 in these experiments, which accounts for the 96% fluorescence quenching observed in Figure 4. Heme, in the absence of protein, did not quench the fluorescence of SC58076 (not shown).

Energy Transfer Analysis of SC58076 Bound to PGHS-1: Determination of the Overlap Integral. Fluorescence resonance energy transfer (FRET) analysis can be used to determine distances between a donor (SC58076) and an acceptor (heme). The fluorescence quenching efficiency is directly related to the distance between heme and SC58076 and can be determined by both steady-state and time-resolved fluorescence spectroscopy. One variable used in calculating the distance between a donor/acceptor pair is the overlap integral, *J*, of the donor emission and acceptor absorbance.

Figure 5 displays the emission spectrum of SC58076 bound to apo PGHS-1 and the absorbance spectrum of the heme of holo PGHS-1. From the equations described in Materials and Methods, the integral of the overlapping region was determined to be 8.28×10^{14} M^{-1} cm^{-1} nm^4. This value is typical for transfer to a heme acceptor and includes a correction for the percentage of PGHS-1 that does not bind heme (*36*).

Determination of Quantum Yields. Other variables necessary to calculate the distance between a donor/acceptor pair are the quantum yields of the donor in the presence (SC58076 bound to holo-PGHS-1) and absence of the acceptor (SC58076 bound to apo-PGHS-1). Because quinine sulfate has very similar absorbance and emission spectra to SC58076, quinine sulfate was used as a reference standard to determine the quantum yields of SC58076 bound to apo- and holo-PGHS-1. The quantum yield of SC58076 bound to apo-PGHS-1 was determined to be 0.78. In contrast, the quantum yield of SC58076 bound to holoprotein was 0.07. The quantum yields were used to determine that the transfer efficiency between SC58076 and the heme of holo-PGHS-1 was 80−90%.

Estimation of κ^2. A final variable necessary to determine the distance between SC58076 and the heme of PGHS-1 is the orientation factor, κ^2. For chromophores that are spheres or behave as spheres and diffuse through all possible orientations, κ^2 has an average value of $^2/_3$. In our system, the heme prosthetic group is considered to have a planar transition moment (*37*), but the fluorophores, SC58076 and SC58092, have a linear transition moment (Figure 6). Incorrect values for κ^2 can introduce significant error into the distance calculations (*36*). Thus, we attempted to calculate a better estimate of κ^2 using the crystal structure of the protein and molecular modeling.

Using the coordinates of PGHS-1, we docked SC58076 into the cyclooxygenase active site. We made use of the fact that SC58076 and SC58092 differ only in the oxidation state of a sulfur atom and that the structure of PGHS-1 differs very little from that of PGHS-2 in the cyclooxygenase active

[2] C. Lanzo, unpublished result.

FIGURE 6: Stereo diagram of the fluorescence dipole of SC58076 and the acceptor dipole of the heme of PGHS-1.

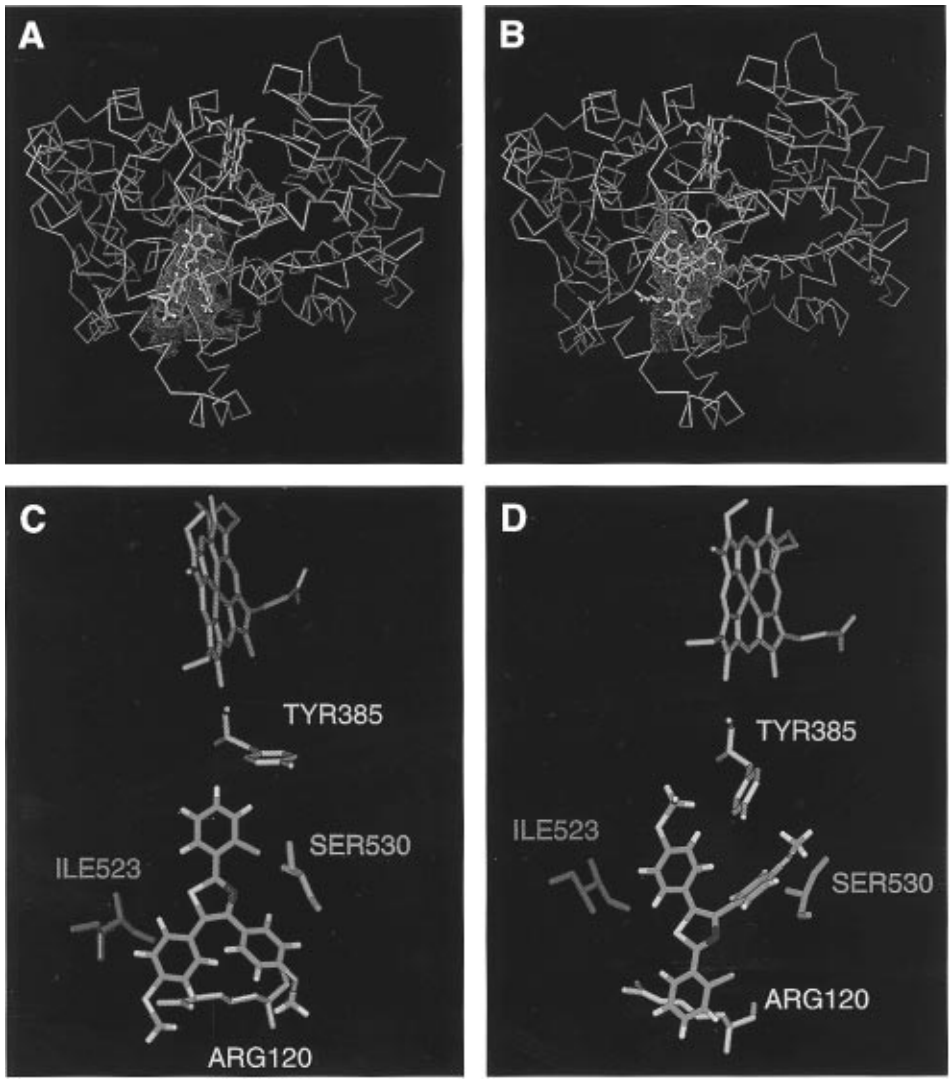

FIGURE 7: Proposed models of SC58076 binding to PGHS-1. (A) SC58076 is situated such that the chlorophenyl group is directed toward Tyr385. $\kappa^2 = 0.1$. (B) SC58076 is situated such that the chlorophenyl group is directed toward the constriction site formed by Tyr355 and Arg120. $\kappa^2 = 0.034$. (C) Trace diagram of PGHS-1 with SC58076 in the orientation described in panel A. (D) Trace diagram of PGHS-1 with SC58076 in the orientation described in panel B. The Connelly surface of the cyclooxygenase channel immediately surrounding the inhibitor is shown in pink. For all views, Tyr385 is in orange, Ile523 is in pink, Arg120 is in yellow, Ser530 is in blue, and the heme is in red.

site. One distinctive difference is that Ile523 in PGHS-1 is a Val in PGHS-2. Mutation of Val to Ile in the PGHS-2 structure resulted in a PGHS-2 that was selectively inhibited by PGHS-1 inhibitors (*28*, *38*, *39*). Therefore, we modeled the docked inhibitor such that the sulfur atom was near to or facing the Ile523 residue in PGHS-1. Steric hindrances dominated the fit of the inhibitor in the active site. Various models were energy-minimized and used for estimating κ^2. Several of the minimized orientations resulted in κ^2s that were clearly unreasonable to describe our data and thus were not used. Through an iterative process, two orientations in which the κ^2 calculation resulted in calculated distances that matched the distance in the model were developed. These two models are shown in Figure 7, and the two values for κ^2 were estimated to be 0.1 and 0.034. Both models have a rms deviation of 1.5 Å from the original coordinates (*22*).

Determination of the Distance between SC58076 and the Heme of PGHS-1. The distance for 50% energy-transfer, $R_{0,}$ is calculated using the index of refraction of the medium (n), the quantum yield of the donor (κ^2), and the overlap integral. With the values we determined and n equal to 1.4, the R_0 was found to be 33 Å ($\kappa^2 = 0.1$) or 28 Å ($\kappa^2 = 0.034$) for PGHS-1 with SC58076. The transfer efficiency and R_0 were then used to determine the distance from the heme to

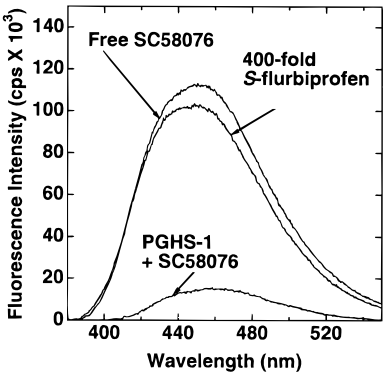

FIGURE 8: Steady-state fluorescence spectroscopy of *S*-flurbiprofen competition with SC58076 for binding to PGHS-1. PGHS-1 (4 μM) was incubated with 400 μM *S*-flurbiprofen for 30 min before the addition of 1 μM SC58076. Fluorescence emission spectra were collected from 380 to 550 nm by exciting samples at 346 nm. Backgrounds were subtracted. The excitation and emission bandwidths were 1−2 nm for all spectra.

SC58076, *R*, as 22 Å ($\kappa^2 = 0.1$) or 19 Å ($\kappa^2 = 0.034$) for steady-state measurements. In agreement with steady-state analysis, global analysis of time-resolved measurements indicated a transfer efficiency equal to 90% and a distribution of distances of 20−28 Å between SC58076 and the heme of PGHS-1. This distance is in close agreement with either one of our models. In Figure 7A,C, the κ^2 is 0.1, and the distance in the model is 21 Å. In Figure 7B,D, the κ^2 is 0.034, and the distance in the model is 18 Å.

Flurbiprofen Competes with SC58076 for Binding PGHS-1. The three-dimensional structure of PGHS-1 was solved with *S*-flurbiprofen bound in the arachidonate binding site (*22*). *S*-Flurbiprofen, end-to-end, is 10−25 Å from the heme. Thus, the calculated distance of SC58076 to the heme of PGHS-1 is similar to the distance of *S*-flurbiprofen to the heme. To determine if SC58076 was binding in the arachidonate binding site, *S*-flurbiprofen was incubated with holo-PGHS-1 before the addition of SC58076. Figure 8 displays steady-state results showing that fluorescence quenching of SC58076 by holo-PGHS-1 is prevented by preincubation with *S*-flurbiprofen. In further support of these findings, time-resolved analysis of the lifetime of SC58076 competed off the enzyme by *S*-flurbiprofen demonstrated SC58076 is only slightly quenched over SC58076 in the presence of *S*-flurbiprofen alone with lifetimes of 0.31 and 0.41 ns, respectively (data not shown). The fluorescence intensity of SC58076 bound to holo-PGHS-1 and competed with *S*-flurbiprofen does not completely return to the intensity observed for free SC58076 because a small fraction remains bound and quenched. Anistropy analysis further shows that SC58076 is no longer bound to PGHS-1 when competed with *S*-flurbiprofen (data not shown).

Stopped-Flow Measurement of SC58076 Competed off Holo-PGHS-1 by S-Flurbiprofen. We measured binding kinetics of SC58076 to holo-PGHS-1 using stopped-flow techniques. We also measured the off rates of SC58076 when competed with *S*-flurbiprofen using stopped-flow techniques. Figure 9 (top) displays the results when SC58076 was rapidly mixed with holo-PGHS-1 (see also Table 1). The on rate is multiexponential and zero-order with respect to SC58076 (data not shown). The spectral changes detected after rapid mixing of holo-PGHS-1, prebound to SC58076,

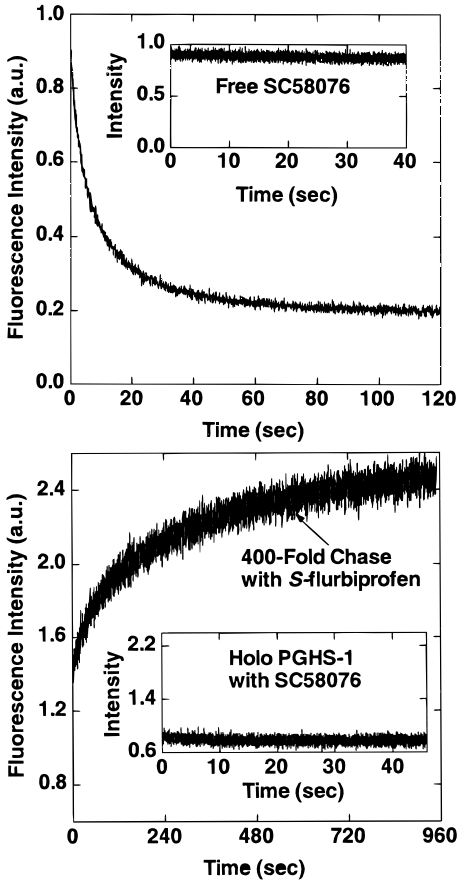

FIGURE 9: On and off rates of SC58076 with PGHS-1 as determined by stopped-flow spectroscopy (Top) Holo-PGHS-1 (4 μM) was rapidly mixed with 500 nM SC58076 to measure the on rate. The inset is SC58076 rapidly mixed with the buffer in which the protein is prepared. (Bottom) PGHS-1 (4 μM) was incubated with 500 nM SC58076 for 20 min. *S*-Flurbiprofen (200 μM) was rapidly mixed with PGHS-1 preloaded with SC58076 to measure the off rate. The inset is holo-PGHS-1 prebound with SC58076 and rapidly mixed with the buffer used for *S*-flurbiprofen. The rates were determined using GLOBALS UNLIMITED software. Fluorescence detection was performed as described in Materials and Methods.

Table 1: Rate Constants for Association and Dissociation of PGHS-1 + SC58076

reaction	k_1[a]	k_2[a]	k_3[a]	χ^2
on rates for PGHS1 + SC58076	1.3	0.22	0.05	0.60×10^{-4}
off rates for PGHS1:SC58076 competed out by *S*-flurbiprofen	0.30	0.05	0.008	0.66×10^{-4}

[a] Units for k are seconds^{-1}.

with *S*-flurbiprofen clearly demonstrates a measurable increase in the fluorescence intensity over time (Figure 9, bottom). The off rate of SC58076 was analyzed and found also to be multexponential (Table 1). Attempts to fit the data to single or double exponentials were unsuccessful. Both the on and off rate are adequately described by three rates. The fastest component for the on rate is 1.3 s^{-1}. The initial association of the inhibitor to PGHS-1 appears to be diffusion-limited; thus, the faster rate may represent movement of the inhibitor from an initial nonspecific binding site to the mouth of the channel. This fast rate is followed by two slower rates, 0.22 s^{-1} and 0.05 s^{-1}. These rates may represent the movement of the inhibitor from the exterior of the channel to the interior of the channel. Similar to the on rate, the off rate is described by three exponentials, which

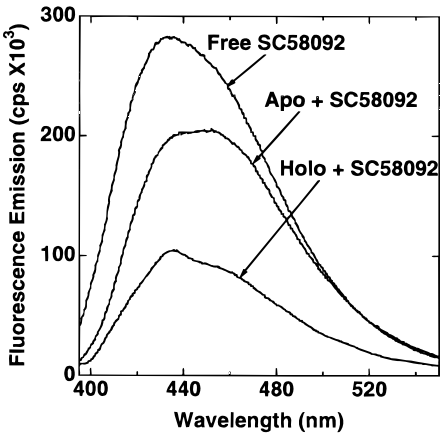

FIGURE 10: Steady-state fluorescence quenching of SC58092 by PGHS-2. PGHS-2 (4 μM) was reconstitituted with 1 equiv of heme or Me_2SO to generate holo- or apoenzyme, respectively. SC58092 (500 nM) was incubated for 20 min with PGHS-2. Backgrounds were subtracted. Emission spectra were recorded as described in Materials and Methods.

may or may not correspond to the reversal of the on rate steps. The off rates are all very slow with 0.3 s^{-1} being the fastest component of the off rate.

Distance of SC58092 from the Heme of PGHS-2. The PGHS-2, selective inhibitor SC58092 has a K_i of 1 μM for PGHS-2 and >100 μM for PGHS-1 (*21*). To determine the distance of SC58092 from the heme of PGHS-2, steady-state analysis was performed in an analogous fashion to the measurements described for PGHS-1. The assumption was made that $\kappa^2 = 0.1$ or 0.034 since the PGHS-2 crystal coordinates were not available in order to perform molecular modeling.

Figure 10 displays the steady-state fluorescence quenching of SC58092 by PGHS-2. SC58092 interacted very differently with PGHS-2 than SC58076 interacted with PGHS-1. Both apo- and holo-PGHS-2 quenched the fluorescence of SC58092. Although the apoenzyme quenched the fluorescence of SC58092 about 20%, we were still able to determine the transfer efficiency of holoenzyme quenching SC58092 relative to apoenzyme with SC58092 as equal to 75%. The overlap integral of the emission spectrum of SC58092 bound to apo-PGHS-2 with the absorbance spectrum of holo-PGHS-2 was equal to 1.03×10^{15} M^{-1} cm^{-1} nm^4 and the quantum yield of the donor, SC58092 bound to apoprotein, was 0.029. The quantum yield of SC58092 when bound to holoprotein and quenched was 0.007. We performed energy transfer analysis on SC58092 interacting with PGHS-2 and determined R_0 to be 20 Å ($\kappa^2 = 0.1$) or 19 Å ($\kappa^2 = 0.034$). The distance from SC58092 to the heme, *R*, was determined to be 17 Å ($\kappa^2 = 0.1$) and 16 Å ($\kappa^2 = 0.034$).

DISCUSSION

This study reports the use of fluorescence quenching to monitor the association of two structurally related but isoform-selective inhibitors of PGHS. SC58076 and SC58092 are diarylthiazoles that are structurally related to compounds currently undergoing human clinical trials for antiinflammatory and analgesic activity (*40*). They contain the same fluorophore and differ only in the oxidation state of the sulfur atom *para* to the thiazole ring. The fluorescence quantum yield of SC58092 is less that that of SC58076, which may result from the electron-withdrawing sulfone substituent. Otherwise, the two molecules are sterically and electronically identical so they are a good pair with which to probe the molecular basis for the selectivity of inhibition of the two enzymes. Our goal has been to better understand how these inhibitors of PGHS-1 and 2 interact with the isoforms to achieve selectivity.

As a first step toward this goal, we characterized the interaction of these isoform-selective, fluorescent inhibitors with their respective PGHS targets. FRET and molecular modeling were employed to determine the distance of isoform-selective inhibitors from the hemes of PGHS-1 and PGHS-2. FRET is an alternative method to X-ray crystallography for studying inhibitor-enzyme complexes and can reveal information about the solution structure of these complexes. Furthermore, one can measure directly the real-time movement of these ligands up the access channel using stopped-flow techniques (Figure 9). We found that protein must contain heme to quench the inhibitor's fluorescence and that the quenching was due to energy transfer to the heme. FRET analyses of steady-state and time-resolved fluorescence measurements revealed the selective inhibitors bind in the cyclooxygenase substrate access channel 18−21 Å from the heme. Binding of these inhibitors to both apo- and holoenzyme was verified by anisotropy measurements. Further, *S*-flurbiprofen prevented binding of these inhibitors by blocking access to the cyclooxygenase active site. This was expected since both molecules inhibit the cyclooxygenase activity but not the peroxidase activity of their respective PGHSs, indicating that they bind in the arachidonic acid binding channel (*21*).

Fluorescence quenching has been used previously to monitor PGHS−inhibitor association by Houtzager et al. (*41*). They monitored the effect of NSAIDs quenching of intrinsic tryptophan fluorescence upon binding to apo PGHS-2. Their conclusions were that the enzyme−inhibitor association followed the classical slow, tight-binding inhibitor model in which there is an initial rapid formation of an equilibrium complex (EI), followed by the slower formation of a tightly bound enzyme−inhibitor complex (EI*) (eq 1). These results are in agreement with a previous study using trypsin resistance to monitor association of inhibitor with apoprotein (*21*). Both the trypsin resistance approach and the fluorescence quenching approach provide information consistent with the conclusions of the kinetic study by Copeland et al. (*34*), which demonstrated that the selectivity for a given isoform derives from a time-dependent association that gives rise to a more tightly bound inhibitor.

The major limitation of monitoring the internal fluorescence of tryptophan residues is that heme quenches the fluorescence so only inhibitor associating with apoprotein can be measured. In addition, FRET measurements to determine distances from the inhibitor to the six potential donor tryptophans is virtually impossible because of the difficulty of deciphering which donor tryptophans fluoresce and which are quenched more efficiently than the remaining tryptophans. Our present work enables distance calculations to be made from a single fluorophore (inhibitor) to a single quencher (heme). Further, our measurements are made with the fluorescent inhibitor binding the catalytically active holoprotein.

Several items had to be established before FRET could be used with our system. First, we determined that neither apoenzyme nor heme alone quenched the fluorescence of SC58076 and that the presence of heme in holoenzyme was required for fluorescence quenching to occur. This is important because it indicates that heme is the energy transfer acceptor and that FRET between SC58076 or SC58092 and the heme can be measured and quantitated. Our titration experiments also demonstrated that bound inhibitor did not prevent heme association. Next, we established that the lack of quenching by apoenzyme was not due to a lack of inhibitor binding the enzyme. In fact, our anisotropy experiments clearly demonstrate that SC58076 binds to both apo- and holoenzyme.

FRET measurements and calculations depend on several other biophysical parameters: (1) the spectral overlap at the wavelengths where fluorescence energy transfer occurs, (2) the quantum yields of the donor in the presence and absence of acceptor, and (3) the orientation factor, κ^2, which describes the relative orientations of the electronic dipoles of the donor and acceptor. Determining the spectral overlap and quantum yields was relatively straightforward, but determination of κ^2 required a rather intensive effort. A default value of $^2/_3$ for κ^2 is often used for FRET. This value is for fluorophores and acceptors that behave as spheres and rotate through all orientations as spheres. In our system, SC58076 and SC58092 are linear donors and heme is a planar acceptor (*33, 37*); thus, the default value of $^2/_3$ for κ^2 is clearly inappropriate. To determine κ^2, we positioned the inhibitor in the cyclooxygenase substrate access channel and energy-minimized for an optimum orientation.

Using molecular modeling, we estimated two different values for κ^2 that result in distances consistent with our data and our model. In one model, κ^2 is 0.1 and the chlorophenyl group of the inhibitor is pointing up at Tyr385 (Figure 7A). In the other model, κ^2 is 0.034 and the chlorophenyl group of the inhibitor is near Arg120 (Figure 7B). The modeling of the binding of SC58076 to PGHS-1 was limited by steric hindrance, and the residues in the binding site had to shift to allow access for the large inhibitor although the shifting only resulted in a 1.5 Å rms deviation from the starting coordinates, demonstrating that the protein maintained overall secondary structure (*22*). In Figure 7A, SC58076 is situated such that the chlorophenyl ring is almost perpendicular to Tyr385. The methyl of the methyl sulfide is 3.3 Å from both the guanidinium group of Arg120 and the hydroxyl of Tyr355. The central heterocyclic ring is 3.9 Å from Ser530, and the ring with the sulfide is 3 Å from Ile523. In the second model, shown in Figure 7B, SC58076 is flipped roughly 180° relative to Figure 7A, and the chlorophenyl ring is facing toward the membrane binding domain and is approximately 3.5 Å from Tyr355 and 5.0 Å from Arg120. The ring with the sulfide is 6 Å from Ile523 and 7 Å from Tyr385. The ring with the methoxy is 4 Å from Ser530.

Our results are in agreement with the X-ray structures of PGHS-1−inhibitor complexes, which have shown that the inhibitors bind in the cyclooxygenase active site, thus blocking access of arachidonic acid to the putative catalytic residue Tyr385 (*22, 23, 42*). The carboxylate moieties of *S*-flurbiprofen, iodosuprofen, and iodoindomethacin ion-pair with Arg120, which provides an anchor for their interaction in the cyclooxygenase active site (*23*). Bromoacetylsalicyclic acid, an aspirin analogue, reacts with PGHS-1, resulting in bromoacetylation of Ser530 and ion-pairing of the displaced salicylate moiety to Arg120 (*43*).

The crystal structures of PGHS-2 complexed with different classes of inhibitors have recently been solved (*26, 27*). The inhibitors bound to PGHS-2 include a diarylheterocycle which is bound in the same site that we calculate for SC58092 (*27*). The conformation of the sulfonamide-containing inhibitor is such that the sulfonamide inserts into a pocket in the substrate access channel bounded by Val509. Such a conformation is not available to SC58076 when it interacts with PGHS-1 because Ile523 blocks access to this pocket. Thus, the structures depicted in Figure 7 are the only currently available models for the binding of a diaryl-heterocycle to PGHS-1.

The interaction of SC58092, the PGHS-2-selective inhibitor, with PGHS-2 seems to be similar to that of SC58076 with PGHS-1. One major difference is that SC58092 is quenched approximately 20% by the apoprotein. This means that there is an interaction with the non-heme-containing protein that results in a small amount of fluorescence quenching that is not due to energy transfer to the heme. We make the assumption that the quenching observed with the apoprotein is also occurring with the holoprotein and, thus, the additional quenching due to the energy transfer to the heme can be quantitated and a distance measurement can be made. Because the crystal coordinates were not available to us for PGHS-2, we used the same values for κ^2 that we calculated for PGHS-1 with SC58076. The distance to the heme from SC58092 when bound to PGHS-2 was determined to be 16−17 Å. This indicates that SC58092 binds in the same site and at approximately the same distance from the heme on PGHS-2 as does SC58076 on PGHS-1. This agrees with the recently solved structures of PGHS-2−inhibitor complexes, which demonstrate that cyclooxygenase inhibitors bind in the same site on PGHS-2 as do the inhibitors on PGHS-1. Despite the agreement between the fluorescence quenching and crystallography results, it is important to point out that the heme−inhibitor distances calculated for PGHS-2 by FRET are estimates based on analogy to PGHS-1 and should only be considered tentative.

The time course for quenching, which occurs over 15−240 s, correlates to the time course of inhibition of the cyclooxygenase activity. Interestingly, the finding that *S*-flurbiprofen displaces the inhibitors from the active site implies that exchange is possible and that it can actually occur at a high rate. This is in contrast to the belief that inhibitors of cyclooxygenase are functionally irreversible. The experiments on which this conclusion is based were performed by dialysis where there is no driving force for the inhibitor to diffuse from the protein because of poor solubility in the dialysis buffer (*34*). In our experiments, exchange was seen by setting up competition with a large excess of *S*-flurbiprofen so inhibitor molecules leaving the binding channel could not reassociate. Indeed, anistropy experiments demonstrate that SC58076, displaced by *S*-flurbiprofen, is no longer bound to the protein.

The present study establishes parameters for the use of fluorescence quenching to monitor association of selective inhibitors with their respective PGHS targets. Our system allows us to measure dynamic events by monitoring the real-time binding of fluorescent inhibitors using stopped-flow

techniques. These fluorescence studies can be validated by comparision to the PGHS crystal structures. The fluorescence data complement the results of crystallography in that the crystal structures give a static picture of inhibitor association in the crystal but cannot provide information about the kinetics of association and the residues in the substrate access channel that determine the kinetics. There are multiple opportunities for the use of fluorescence quenching to monitor dynamics of inhibitor−enzyme association, and we have provided preliminary data demonstrating the utility of this approach.

ACKNOWLEDGMENT

We are grateful to R. M. Garavito for the coordinates of PGHS-1. We thank Jason Sutin for his helpful discussions in estimating κ^2 and in preparation of figures 6 and 7, Diane Denson for assistance in preparing PGHS-1, and J. Gierse for providing samples of PGHS-2.

REFERENCES

1. Van Der Ouderaa, F. J., Buytenhek, M., Slikkerveer., F. J., and Dorp, D. A. V. (1979) *Biochim. Biophys. Acta 109*, 1−8.
2. Sirois, J., and Richards, J. S. (1992) *J. Biol. Chem. 267*, 6382−6388.
3. Fletcher, B. S., Kujubu, D. A., Perrin, D. M., and Herschman, H. R. (1992) *J. Biol. Chem. 267*, 4338−4344.
4. Hamberg, M., Svensson, J., Wakabayashi, T., and Samuelsson, B. (1974) *Proc. Natl. Acad. Sci. U.S.A. 71*, 345−349.
5. Nugteren, D. H., and Hazelhof, E. (1973) *Biochim. Biophys. Acta 326*, 448−461.
6. Xie, W. L., Chipman, J. G., Robertson, D. L., Erickson, R. L., and Simmons, D. L. (1991) *Proc. Natl. Acad. Sci. U.S.A. 88*, 2692−2696.
7. Hla, T., and Neilson, K. (1992) *Proc. Natl. Acad. Sci. U.S.A. 89*, 7384−7388.
8. Kujubu, D. A., Reddy, S. T., Fletcher, B. S., and Herschman, H. R. (1993) *J. Biol. Chem. 268*, 5425−5430.
9. Kujubu, D. A., Fletcher, B. S., Varnum, B. C., Lim, R. W., and Herschman, H. R. (1991) *J. Biol. Chem. 266*, 12866−12872.
10. O'Banion, M. K., Sadowski, H. B., Winn, V., and Young, D. A. (1991) *J. Biol. Chem. 265*, 16737−16740.
11. Masferrer, J. L., Zweifel, B. S., Manning, P. T., Hauser, S. D., Leahy, K. M., Smith, W. G., Isakson, P. C., and Seibert, K. (1994) *Proc. Natl. Acad. Sci. U.S.A. 91*, 3228−3232.
12. Peri, K. G., Hardy, P., Li, D. Y., Varma, D. R., and Chemtob, S. (1995) *J. Biol. Chem. 270*, 24615−24620.
13. Vane, J. R. (1971) *Nature (New Biol.) 231*, 232−234.
14. Meade, E. A., Smith, W. L., and DeWitt, D. L. (1993) *J. Biol. Chem. 268*, 6610−6614.
15. Mitchell, J. A., Akarasereenont, P., Thiermermann, C., Flower, R. J., and Vane, J. R. (1994) *Proc. Natl. Acad. Sci. U.S.A. 90*, 11693−11697.
16. Gans, K. R., Galbraith, W., Roman, R. J., Haber, S. B., Kerr, J. S., Schmidt, W. K., Smith, C., Hewes, W. E., and Ackerman, N. R. (1990) *J. Pharmacol. Exp. Ther. 254*, 180−187.
17. Futaki, N., Yoshikawa, K., Hamasaka, Y., Arai, I., Higuchi, S., Iizuka, H., and Otomo, S. (1993) *Gen. Pharmacol. 24*, 105−110.
18. Reitz, D. B., Li, J. J., Norton, M. B., Reinhard, E. J., Huang, H.-C., Penick, M. A., Collins, J. T., Garland, D. J., Seibert, K., Koboldt, C. M., Gregory, S. A., Veenhuizen, A. W., Zhang, Y., and Isakson, P. C. (1994) *J. Med. Chem. 38*, 4570−4578.
19. Reitz, D. B., Huang, H.-C., Li, J., Garland, D. J., Manning, R. E., Anderson, G. D., Gregory, S. A., Koboldt, C. M., Perkins, W., Seibert, K., and Isakson, P. C. (1995) *Bioorg. Med. Chem. Lett. 5*, 867−872.
20. Kennedy, T. A., Smith, C. J., and Marnett, L. J. (1994) *J. Biol. Chem. 269*, 27357−27364.
21. Kalgutkar, A. S., Crews, B. C., and Marnett, L. J. (1996) *Biochemistry 35*, 9076- 9082.
22. Picot, D., Loll, P. J., and Garavito, R. M. (1994) *Nature 367*, 243−249.
23. Loll, P. J., Picot, D., Ekabo, O., and Garavito, R. M. (1996) *Biochemistry 35*, 7330−7340.
24. Mancini, J. A., Riendeau, D., Falgueyret, J.-P., Vickers, P. J., and O'Neill, G. P. (1995) *J. Biol. Chem. 270*, 29372−29377.
25. Bhattacharyya, D. K., Lecomte, M., Rieke, C. J., Garavito, R. M., and Smith, W. L. (1996) *J. Biol. Chem. 271*, 2179−2184.
26. Luong, C., Miller, A., Barnett, J., Chow, J., Ramesha, C., and Browner, M. F. (1996) *Nat. Struct. Biol. 3*, 927−933.
27. Kurumbail, R. G., Stallings, W. C., Mcdonald, J. J., Stevens, A. M., Stegeman, R. A., Pak, J. Y., Gildehaus, D., Gierse, J. K., Miyashiro, J. M., Penning, T. D., Seibert, K., and Isakson, P. C. (1996) *Nature 384*, 644−648.
28. Gierse, J. K., Mcdonald, J. J., Hauser, S. D., Rangwala, S. H., Koboldt, C. M., and Seibert, K. (1996) *J. Biol. Chem. 271*, 15810−15814.
29. Marnett, L. J., Siedlik, P. H., Ochs, R. C., Pagels, W. D., Das, M., Honn, K. V., Warnock, R. H., Tainer, B. E., and Eling, T. E. (1984) *Mol. Pharmacol. 26*, 328−335.
30. Odenwaller, R., Chen, Y.-N. P., and Marnett, L. J. (1990) *Methods Enzymol. 187*, 479−485.
31. Beechem, J. M., Gratton, E., Ameloot, M., Knutson, J. R., and Brand, L. (1991) in *Topics in Fluorescence Spectroscopy* (Lackowicz, J. R., Ed.) Vol. 2, Plenum Press, New York.
32. Rao, A., Martin, P., Reithmeier, R. A. F., and Cantley, L. C. (1979) *Biochemistry 18*, 4505−4516.
33. Gudipati, M. S., Maus, M., Daverkausen, J., and Hohlneicher, G. (1995) *Chem. Phys. 192*, 37−47.
34. Copeland, R. A., Williams, J. M., Giannaras, J., Nurnberg, S., Covington, M., Pinto, D., Pcik, S., and Trazaskos, J. M. (1994) *Proc. Natl. Acad. Sci. U.S.A. 91*, 11202−11206.
35. Chen, Y.-N. P., Bienkowski, M. J., and Marnett, L. J. (1987) *J. Biol. Chem. 262*, 16892−16899.
36. Wieb Van Der Meer, B. E. C., III, and Chen, S.-Y. (1994) *Resonance Energy Transfer Theory and Data*, VCH Publishers, Inc., New York.
37. Gryczynski, Z., Tenenholz, T., and Bucci, E. (1992) *Biophys. J. 63*, 648−653.
38. Guo, Q., Wang, L.-H., Ruan, K.-H., and Kulmacz, R. J. (1996) *J. Biol. Chem. 271*, 19134−19139.
39. Wong, E., Bayly, C., Waterman, H., Riendeau, D., and Mancini, J. (1997) *J. Biol. Chem. 272*, 9280−9286.
40. Penning, T. D., Talley, J. J., Bertenshaw, S. R., Carter, J. S., Collins, P. W., Doctor, S., Graneto, M. J., Lee, L. F., Malecha, J. W., Miyashiro, J. M., Rogers, R. S., Rogiers, D. J., Yu, S. S., Anderson, G. D., Burton, E. G., Cogburn, J. N., Gregory, S. A., Koboldt, C. M., Perkins, W. E., Seibert, K., Veenhuizen, S. W., Zhang, Y. Y., and Isakson, P. C. (1997) *J. Med. Chem. 40*, 1347−1365.
41. Houtzager, V., Ouellet, M., Falgueyret, J.-P., Passmore, L. A., Bayly, C., and Percival, M. D. (1996) *Biochemistry 35*, 10974−10984.
42. Shimokawa, T., Kulmacz, R. J., DeWitt, D. L., and Smith, W. L. (1990) *J. Biol. Chem. 265*, 20073−20076.
43. Loll, P. J., Picot, D., and Garavito, R. M. (1995) *Nat. Struct. Biol. 2*, 637−643.
44. Velapoldi, R. A. (1972) *J. Res. Natl. Bur. Stand. (U.S.) 76A*, 641−654.

BI971691N